


Experimental Observation of Exchange-Driven Chiral Effects in Curvilinear MagnetismOleksii M. Volkov,^{1,*} Attila Kákay,¹ Florian Kronast,² Ingolf Mönch,¹ Mohamad-Assaad Mawass,²
Jürgen Fassbender,¹ and Denys Makarov^{1,†}¹*Helmholtz-Zentrum Dresden-Rossendorf e.V., Institute of Ion Beam Physics and Materials Research, 01328 Dresden, Germany*²*Helmholtz-Zentrum Berlin für Materialien und Energie, 12489 Berlin, Germany* (Received 30 April 2019; published 15 August 2019)

The main origin of the chiral symmetry breaking and, thus, for the magnetochiral effects in magnetic materials is associated with an antisymmetric exchange interaction, the intrinsic Dzyaloshinskii-Moriya interaction (DMI). Recently, numerous inspiring theoretical works predict that the bending of a thin film to a curved surface is often sufficient to induce similar chiral effects. However, these originate from the exchange or magnetostatic interactions and can stabilize noncollinear magnetic structures or influence spin-wave propagation. Here, we demonstrate that curvature-induced chiral effects are experimentally observable rather than theoretical abstraction and are present even in conventional soft ferromagnetic materials. We show that, by measuring the depinning field of domain walls in the simplest possible curve, a flat parabolic stripe, the effective exchange-driven DMI interaction constant can be quantified. Remarkably, its value can be as high as the interfacial DMI constant for thin films and can be tuned by the parabola's curvature.

DOI: [10.1103/PhysRevLett.123.077201](https://doi.org/10.1103/PhysRevLett.123.077201)

Broken magnetic symmetry is a key aspect in condensed matter physics and, in particular, in magnetism. It can lead to the appearance of chiral effects, such as the topological Hall effect [1], or to the formation of chiral noncollinear magnetic textures, as skyrmions [1–3] and chiral domain walls (DWs) [4,5]. These chiral structures can be the key components for realizing novel concepts for magnonics [6], antiferromagnetic spintronics [7], spin-orbitronics [8,9], and oxitronics [10,11]. So far, the main chiral symmetry breaking effects considered as being the origin for the presence of chiral noncollinear magnetic textures are the exchange frustration [12] and the intrinsic Dzyaloshinskii-Moriya interaction (DMI) [13,14]. The latter, an antisymmetric exchange interaction, can develop in certain magnetic crystals in which the unit cell lacks inversion symmetry, such as the gyrotropic magnetic crystals [13,14], or appear typically in ultrathin films or bilayers due to the inversion symmetry breaking on the film interface [15–17]. At present, tailoring of DMI is done by optimizing materials, either doping a bulk single crystal [18,19] or adjusting interface properties of thin films and multilayers [20]. A viable alternative to the tuning of the intrinsic properties of materials can be the break of local inversion symmetry appearing in curvilinear structures of conventional materials [21–23]. Magnetic switching processes in curved nanostripes [24–26] and nanorings [27–29] are studied experimentally primarily to address DW dynamics for prospective memory [30–32] and logic [33–35] devices. Because of considered geometries and dimensions of magnetic structures, these works do not address exchange-driven chiral effects in curvilinear magnets. Therefore, by

now, these novel geometry-driven chiral interactions are investigated only theoretically [36–38]. No experiment is known yet to confirm this exciting theoretical prediction.

Here, we provide the very first experimental confirmation of the existence of the curvature-induced chiral interaction of exchange origin in a conventional soft ferromagnetic material. We experimentally explore the theoretical predictions, that the magnetization reversal of flat parabolic stripes shows a two-step process. At the first switching event, a DW pinned by the curvature-induced exchange-driven DMI is expelled, leading to a magnetization state homogeneous along the parabola's long axis as schematically shown in Fig. 1(a). Measuring the depinning field enables one to quantify the effective exchange-driven DMI constant. The magnitude of the effect can be tuned by the parabola's curvature and width.

Although the curvilinear exchange-driven chiral effects are generic, they are difficult to find in experiments, because they are shaded by other effects or interactions such as the long-range magnetostatic interaction. Moreover, the exchange interaction alone in a curved system will not lead to curvature-induced chiral effects. A further requirement is the existence of an anisotropy which reflects the shape of the curvature. The parabolic stripe geometry is not only the mathematically simplest possible curve with well-defined geometrical properties [Fig. 1(b)] but the ideal object to study the curvature-induced exchange-driven chiral effects. It has a *curvature gradient* that forms a potential well for the pinning of a possible chiral magnetic texture [39]. The *anisotropy* reflecting the shape is present by default because of the magnetostatic interaction as a shape anisotropy. Moreover,

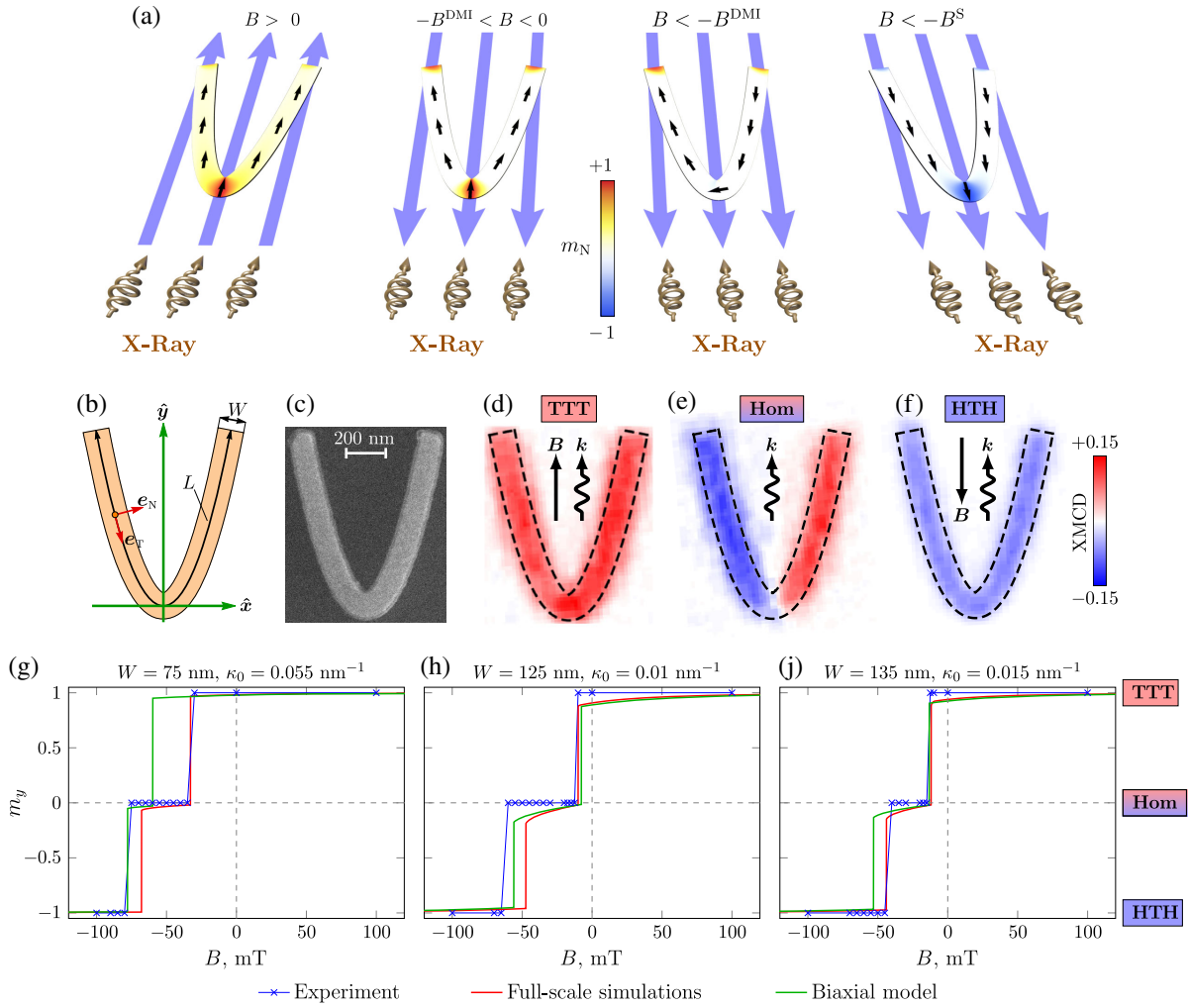


FIG. 1. Hysteresis loops and states. (a) Schematic illustration of the four main magnetic states appearing during the field reversal: saturation, domain wall (head-to-head or tail-to-tail), homogeneous along the parabola, and again saturation in the reversed field. The blue arrows mark the external field direction, and the small black arrows indicate the magnetization direction. In color code, the component of the magnetization perpendicular to the parabola's long axis is shown. Reducing the field from positive saturation to zero, a DW is forming at the apex of the parabolic stripe. In order to remove the DW pinned by the curvature-induced DMI at the apex, a certain negative field $-B^{\text{DMI}}$ has to be applied. Further increasing the field in the negative direction at B^{S} , a DW will nucleate at the end of the parabola and move into the apex, thus reversing the magnetization. (b) Schematic picture of a parabolic stripe construction. Green arrows correspond to the Cartesian frame of references, while red ones refer to a local curvilinear frame of references. (c) Scanning electron microscopy image of a patterned stripe with $L = 2 \mu\text{m}$ length, $W = 135 \text{ nm}$ width, and $\kappa_0 = 0.015 \text{ nm}^{-1}$ vertex curvature. The main magnetic states imaged by XMCD-PEEM appearing during the field reversal are (d) tail-to-tail (TTT) DW, (e) homogeneous along the parabola, and (f) head-to-head (HTH) DW. A comparison of experimentally and numerically obtained hysteresis loops for parabolic stripes are shown for the following stripe widths: (g) $W = 135 \text{ nm}$ and $\kappa_0 = 0.015 \text{ nm}^{-1}$, (h) $W = 75 \text{ nm}$ and $\kappa_0 = 0.05 \text{ nm}^{-1}$, and (j) $W = 125 \text{ nm}$ and $\kappa_0 = 0.01 \text{ nm}^{-1}$. Blue crosses correspond to the experimentally observed magnetic contrast change via the XMCD-PEEM imaging. Red lines correspond to results of the full-scale micromagnetic simulations.

due to the flatness of the parabolas, the *magnetostatic-driven curvilinear effects* can be neglected. These are the right ingredients which push exchange-driven chiral effects to the forefront and enable their experimental validation.

Parabolic stripes with 10-nm-thick $\text{Ni}_{81}\text{Fe}_{19}$ (permalloy, Py) and various geometrical parameters (stripe length $L = 2 \mu\text{m}$, width $W = 75\text{--}135 \text{ nm}$, and vertex curvature $\kappa_0 = 0.005\text{--}0.07 \text{ nm}^{-1}$) were patterned using electron-beam lithography and ion beam etching [Fig. 1(c)]; see

Sec. S1 in Ref. [40]. The static magnetization states appearing during hysteresis loops are visualized with x-ray magnetic circular dichroism photoelectron emission microscopy (XMCD-PEEM) [Figs. 1(d)–1(f)]. Parallel, perpendicular, and antiparallel alignment of the magnetization with respect to the x-ray beam direction is encoded by a red-white-blue color scheme. As shown in Figs. 1(d)–1(f), two switching events separated by a plateau region can be distinguished while reversing the external field (the blue crosses are the

experimental data); see Sec. S2 in Ref. [40]. Note, in all considered geometries, Figs. 1(g)–1(j) show the same two-step switching.

To understand this two-step switching process, full-scale finite element micromagnetic simulations are performed for parabolic stripes with geometrical parameters taken from the experiment; see Sec. S3 in Ref. [40]. The resulting hysteresis loops are shown in Figs. 1(g)–1(j) as red solid lines. The specific two-step switching process with three easily identifiable plateaus is present for all considered geometries. Each of the plateaus refers to stable magnetic states: tail-to-tail and head-to-head domain walls and a homogeneous magnetic state along the parabolic stripe (middle plateau). Analyzing the simulations at the first switching field B^{DMI} , indeed the tail-to-tail DW is depinned from the parabola apex and propagates along one of the parabolic branches, leading to the appearance of the homogeneous magnetic state. The second switching field B^S is related to the nucleation of a head-to-head DW from the end of a parabolic branch and its propagation into the apex area. Remarkably, the simulation results concerning B^{DMI} are in perfect agreement with the experimentally measured ones, while the results for the second switching field reveal a quantitative discrepancy. This already suggests that the sample imperfections, due to the patterning, do not influence the DW dynamics at the first switching but make a significant influence on a DW nucleation process.

To define the fundamental influence of the exchange and the magnetostatic interactions on switching processes, additional micromagnetic simulations are performed using a local magnetostatic model in which the magnetostatic interaction is replaced by a biaxial shape anisotropy composed of an easy plane and uniaxial terms [49]; see Secs. S3 and S4 in Ref. [40]. Corresponding hysteresis loops for three investigated parabolic geometries are shown in Figs. 1(g)–1(j) as green solid lines. While the resulting hysteresis loops reveal the qualitatively same two-step switching process, which was discussed above, for two wide parabolic stripes ($W = 125$ and 135 nm) the first switching fields have a quantitative match with both experimental and full-scale micromagnetic hysteresis loops. The quantitative discrepancies in the second switching fields are present for all studied geometries. It is well known from the literature that the B^S field is magnetostatic driven and has been extensively studied in the case of rectilinear geometries [50,51]. The obtained discrepancy in the first switching fields for several parabolic stripes ($W = 75$ nm, $\kappa_0 = 0.055$ nm $^{-1}$) appears due to the local widening of the apex area for parabolic stripes with big curvatures; see Sec. S2 in Ref. [40]. This widening leads to the local change of the shape anisotropy, which is not taken into account in the biaxial model. The good agreement of the depinning fields compared to those obtained from the full-scale micromagnetic simulations in the unshaded region ensures that the biaxial anisotropy model is a valid

approximation for such flat parabolic stripes. Moreover, it demonstrates that the magnetostatic-driven curvilinear effect can be neglected when describing the first switching field.

To determine the influence of the apex curvature κ_0 on the DW pinning, additional full-scale simulations are performed for parabolic stripes with a constant width but varying curvature as shown in Fig. S4 in Ref. [40]. In Fig. 2, the dependence of the DW depinning field B^{DMI} as a function of the curvature κ_0 is summarized for stripes with four different widths. The shaded areas represent parabolic stripe geometries with local widening in the apex region. The depinning field increases with the decrease of the stripe width and increase of the parabolic curvature. The $B^{\text{DMI}}(\kappa_0)$ dependence reveals the presence of two linear trends with an intermediate nonlinear transition region. Such a change in the dependence trend indicates the transition from the exchange-induced to the magnetostatically-induced curvilinear effects in the DW depinning processes. To demonstrate this, we simulate parabolic nanostripes with different κ_0 in the framework of the biaxial model; see the green curves in Fig. 2. The resulting $B^{\text{DMI}}(\kappa_0)$ dependence reveals only one linear trend, which

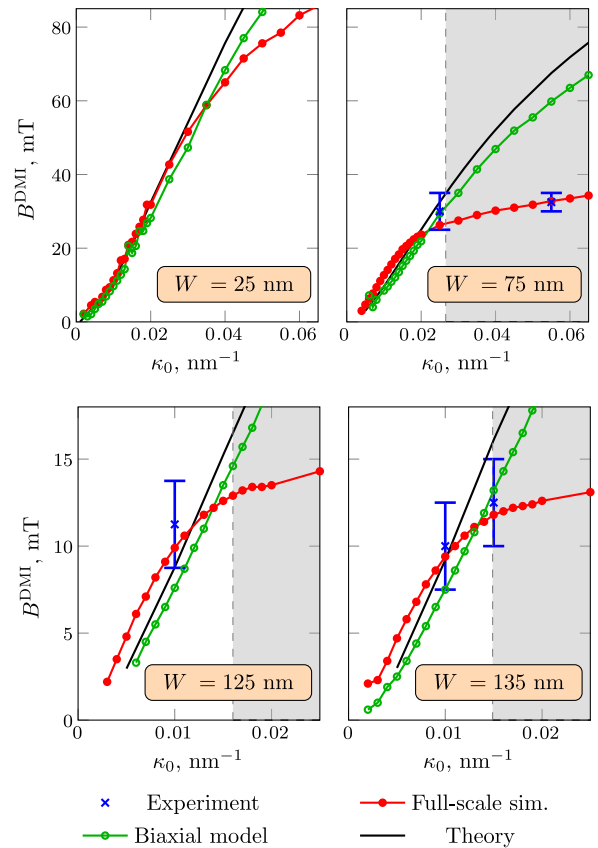


FIG. 2. Dependence of the DW depinning field on the curvature. Depinning fields as a function of the vertex curvature are shown for parabolic stripes with the following widths: 25, 75, 125, and 135 nm.

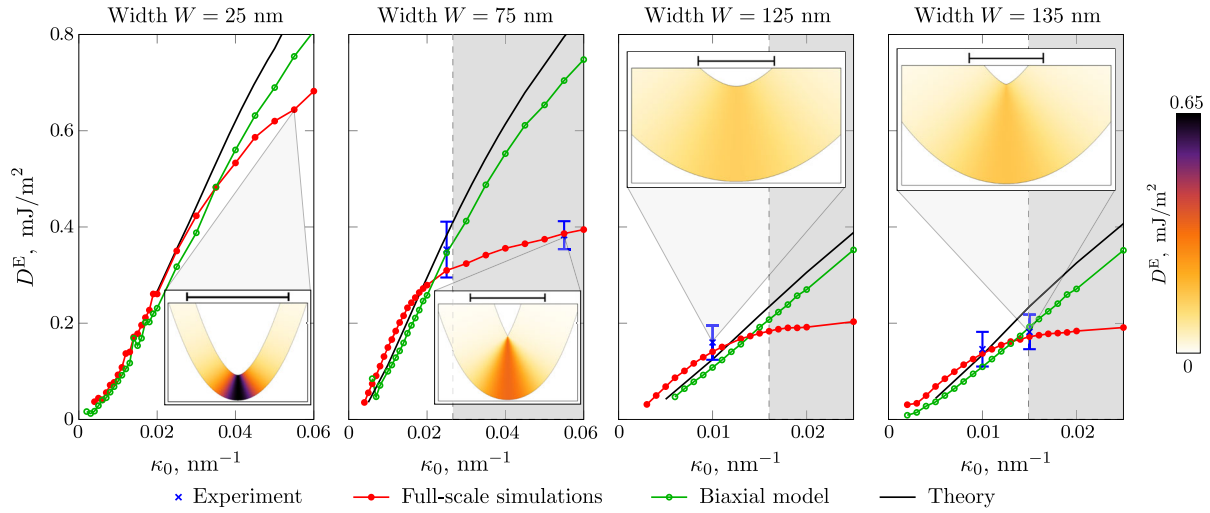


FIG. 3. Exchange-driven effective DMI constant. Dependencies of the exchange-driven DMI D^E constants on curvature κ_0 for different parabolic stripe widths. Results show that its value can be tuned over a broad interval by tailoring the apex curvature. The inset pictures represent the distribution of the D^E along the parabolic stripe apex. Scale bars correspond to 100 nm for all the inset pictures.

is almost the same as the first linear trend obtained from the full-scale micromagnetic simulations. Thus, this assures that the source of the geometrical pinning potential is the curvature-induced exchange-driven DMI, which was discussed earlier on DW depinning in curvilinear stripes [24,26,52].

To obtain a deeper insight into the origin of the depinning mechanism of the transversal DW, we conducted analytical calculations using the biaxial anisotropy approximation of the magnetostatic interaction for a one-dimensional system [49]; see Sec. S5 in Ref. [40]. In parabolic stripes, the curvature-induced DMI interaction is well localized at the vicinity of the apex, and its vector is perpendicular to the parabolic plane. The theoretical curvature dependence of the depinning fields B^{DMI} are shown as black lines in Fig. 2. The results are in perfect agreement with those obtained by full-scale micromagnetic simulations for small curvatures. The influence of the exchange-induced curvilinear effects on the DW depinning field B^{DMI} is demonstrated by artificially turning on and off the exchange-driven DMI and/or anisotropy terms in the energy functional; see Supplemental Material Sec. S5 [40]. With the induced DMI term set to zero, the initial tail-to-tail DW switched to a homogeneous magnetic state along the stripe at a nearly zero negative field, in large contrast to the experimental and full-scale simulation results. However, the absence of the effective anisotropy term has only a negligible effect on the depinning fields. These results demonstrate that the depinning fields summarized in Fig. 2 for curvatures in the unshaded area originate from the curvature-induced exchange-driven DMI interaction. In the shaded area, usually for large curvatures, the parabolic stripes become wedge shaped, resulting in a local widening of the apex area. This leads to a change of the domain wall profile (see Supplemental Material Secs. S6 and S7 [40]) and

in the modification of the shape anisotropy arising from the magnetostatic interaction.

Using a one-dimensional q - Φ model [39] in the curvilinear frame of references, we analytically determine the energy landscape along the parabolic stripe [see Fig. S7(f) in Sec. S6 in Ref. [40]] as a function of the external field; see Sec. S6 in Ref. [40]. The exchange-driven DMI creates a potential well for the transverse DWs, which are naturally forming during the reversal process. To remove a pinned DW, it is necessary to apply a depinning field B^{DMI} , which modifies the energy landscape such that the DW can move out into one of the parabolic branches. Thus, the experimentally determined values of the DW depinning fields B^{DMI} allow us to make a direct quantitative assessment of the exchange-driven DMI constant:

$$D^E = B^{\text{DMI}} M_s \ell \sqrt{\frac{2\pi W}{H[2 \ln(W/H) + 3]}}, \quad (1)$$

where M_s is the saturation magnetisation and ℓ is the exchange length.

As a final step, we calculate the strength of the exchange-driven DMI constants based on Eq. (1) for all experimental and simulation results. The dependence of D^E on κ_0 for parabolic stripes with different widths is summarized in Fig. 3. Varying the geometrical parameters of the stripe (e.g., W and κ_0), the value of D^E can be tuned in a wide range. Among the experimentally realized geometries, the largest value, namely, ≈ 0.4 mJ/m², is found for the parabolas with $W = 75$ nm and $\kappa_0 = 0.05$ nm⁻¹. Note that this value is comparable with those experimentally reported values obtained for asymmetric Co sandwiches [53] with interfacial DMI. This comparison can be made due to the following reason: The symmetry of the exchange-driven

DMI depends on the geometrical curvatures such that its vector is always perpendicular to the local bending plane [54]. The consequence of this symmetry leads to the stabilization of magnetic textures with a preferred chirality similar to the case of conventional spin-orbit DMI, emergent at interfaces of thin ferromagnetic films and heavy metals [55].

In summary, we have shown that the exchange-driven chiral effects in curvilinear ferromagnets are experimentally observable rather than just theoretical abstraction. Furthermore, we could quantify from the experimental results, supported by micromagnetic simulations and analytics, the strength of the effective exchange-driven DMI constant, which is found to be remarkably strong compared to the surface-induced DMI. Its value can be tuned by tailoring local curvatures and shapes of ferromagnets—in the present case, by the parabola’s curvature. Finally, it should be emphasized that these exchange-driven chiral effects are observable on well-studied “classical” ferromagnets with orders of magnitude larger dimensions than the exchange length and, therefore, do not require exotic materials or special fabrication routines. The presented study legitimates the predictive power of full-scale micromagnetic simulations to design the properties of ferromagnets through their geometry, thus stabilizing chiral textures.

We thank T. Voitsekhivska (HZDR) for assistance in the deposition of permalloy thin films and E. Christalle (HZDR) for SEM measurements. Support by the Ion Beam Center of the HZDR is gratefully acknowledged. We thank HZB for the allocation of synchrotron radiation beamtime. This work was financed in part via the BMBF project GUC-LSE (federal research funding of Germany FKZ: 01DK17007), and German Research Foundation (DFG) Grants No. MA5144/9-1, No. MA5144/13-1, and No. KA5069/1-1.

*o.volkov@hzdr.de

†d.makarov@hzdr.de

- [1] N. Nagaosa and Y. Tokura, Topological properties and dynamics of magnetic skyrmions, *Nat. Nanotechnol.* **8**, 899 (2013).
- [2] A. N. Bogdanov and D. A. Yablonskiĭ, Thermodynamically stable “vortices” in magnetically ordered crystals, The mixed state of magnets, *Zh. Eksp. Teor. Fiz.* **95**, 178 (1989) [*Sov. Phys. JETP* **68**, 101 (1989)].
- [3] A. Fert, N. Reyren, and V. Cros, Magnetic skyrmions: Advances in physics and potential applications, *Nat. Rev. Mater.* **2**, 17031 (2017).
- [4] A. Thiaville, S. Rohart, É. Jué, V. Cros, and A. Fert, Dynamics of Dzyaloshinskii domain walls in ultrathin magnetic films, *Europhys. Lett.* **100**, 57002 (2012).
- [5] S. Emori, U. Bauer, S.-M. Ahn, E. Martinez, and G. S. D. Beach, Current-driven dynamics of chiral ferromagnetic domain walls, *Nat. Mater.* **12**, 611 (2013).
- [6] A. V. Chumak, V. I. Vasyuchka, A. A. Serga, and B. Hillebrands, Magnon spintronics, *Nat. Phys.* **11**, 453 (2015).
- [7] T. Jungwirth, X. Marti, P. Wadley, and J. Wunderlich, Antiferromagnetic spintronics, *Nat. Nanotechnol.* **11**, 231 (2016).
- [8] I. M. Miron, K. Garello, G. Gaudin, P.-J. Zermatten, M. V. Costache, S. Auffret, S. Bandiera, B. Rodmacq, A. Schuhl, and P. Gambardella, Perpendicular switching of a single ferromagnetic layer induced by in-plane current injection, *Nature (London)* **476**, 189 (2011).
- [9] K. Garello, I. M. Miron, C. O. Avci, F. Freimuth, Y. Mokrousov, S. Blügel, S. Auffret, O. Boule, G. Gaudin, and P. Gambardella, Symmetry and magnitude of spin-orbit torques in ferromagnetic heterostructures, *Nat. Nanotechnol.* **8**, 587 (2013).
- [10] M. Bibes and A. Barthélémy, Oxide spintronics, *IEEE Trans. Electron Devices* **54**, 1003 (2007).
- [11] M. Bibes, J. E. Villegas, and A. Barthélémy, Ultrathin oxide films and interfaces for electronics and spintronics, *Adv. Phys.* **60**, 5 (2011).
- [12] A. Yoshimori, A new type of antiferromagnetic structure in the rutile type crystal, *J. Phys. Soc. Jpn.* **14**, 807 (1959).
- [13] I. Dzyaloshinsky, A thermodynamic theory of “weak” ferromagnetism of antiferromagnetics, *J. Phys. Chem. Solids* **4**, 241 (1958).
- [14] T. Moriya, New Mechanism of Anisotropic Superexchange Interaction, *Phys. Rev. Lett.* **4**, 228 (1960).
- [15] A. Crépieux and C. Lacroix, Dzyaloshinsky-Moriya interactions induced by symmetry breaking at a surface, *J. Magn. Magn. Mater.* **182**, 341 (1998).
- [16] M. Bode, M. Heide, K. von Bergmann, P. Ferriani, S. Heinze, G. Bihlmayer, A. Kubetzka, O. Pietzsch, S. Blügel, and R. Wiesendanger, Chiral magnetic order at surfaces driven by inversion asymmetry, *Nature (London)* **447**, 190 (2007).
- [17] H. Yang, A. Thiaville, S. Rohart, A. Fert, and M. Chshiev, Anatomy of Dzyaloshinskii-Moriya Interaction at Co/Pt Interfaces, *Phys. Rev. Lett.* **115**, 267210 (2015).
- [18] A. Fert and P. M. Levy, Role of Anisotropic Exchange Interactions in Determining the Properties of Spin-Glasses, *Phys. Rev. Lett.* **44**, 1538 (1980).
- [19] P. M. Levy and A. Fert, Anisotropy induced by nonmagnetic impurities in CuMn spin-glass alloys, *Phys. Rev. B* **23**, 4667 (1981).
- [20] J. R. Childress, J. L. Duvail, S. Jasmin, A. Barthélémy, A. Fert, A. Schuhl, O. Durand, and P. Galtier, Perpendicular magnetic anisotropy in $\text{Co}_x\text{Pd}_{1-x}$ alloy films grown by molecular beam epitaxy, *J. Appl. Phys.* **75**, 6412 (1994).
- [21] R. Hertel, Curvature-induced magnetochirality, *SPIN* **03**, 1340009 (2013).
- [22] R. Streubel, P. Fischer, F. Kronast, V. P. Kravchuk, D. D. Sheka, Y. Gaididei, O. G. Schmidt, and D. Makarov, Magnetism in curved geometries (topical review), *J. Phys. D* **49**, 363001 (2016).
- [23] A. Fernández-Pacheco, R. Streubel, O. Fruchart, R. Hertel, P. Fischer, and R. P. Cowburn, Three-dimensional nanomagnetism, *Nat. Commun.* **8**, 15756 (2017).
- [24] E. R. Lewis, D. Petit, L. Thevenard, A. V. Jausovec, L. O’Brien, D. E. Read, and R. P. Cowburn, Magnetic domain

- wall pinning by a curved conduit, *Appl. Phys. Lett.* **95**, 152505 (2009).
- [25] G. Nahrwold, L. Bocklage, J. M. Scholtyssek, T. Matsuyama, B. Krüger, U. Merkt, and G. Meier, Current-induced domain-wall depinning in curved permalloy nanowires, *J. Appl. Phys.* **105**, 07D511 (2009).
- [26] S. Glathe and R. Mattheis, Magnetic domain wall pinning by kinks in magnetic nanostripes, *Phys. Rev. B* **85**, 024405 (2012).
- [27] M. Kläui, C. A. F. Vaz, L. J. Heyderman, U. Rüdiger, and J. A. C. Bland, Spin switching phase diagram of mesoscopic ring magnets, *J. Magn. Magn. Mater.* **290291**, 61 (2005).
- [28] K. Richter, A. Krone, M.-A. Mawass, B. Krüger, M. Weigand, H. Stoll, G. Schütz, and M. Kläui, Localized domain wall nucleation dynamics in asymmetric ferromagnetic rings revealed by direct time-resolved magnetic imaging, *Phys. Rev. B* **94**, 024435 (2016).
- [29] M.-A. Mawass, K. Richter, A. Bisig, R. M. Reeve, B. Krüger, M. Weigand, H. Stoll, A. Krone, F. Kronast, G. Schütz, and M. Kläui, Switching by Domain-Wall Automation in Asymmetric Ferromagnetic Rings, *Phys. Rev. Applied* **7**, 044009 (2017).
- [30] M. Hayashi, L. Thomas, C. Rettner, R. Moriya, and S. S. P. Parkin, Direct observation of the coherent precession of magnetic domain walls propagating along permalloy nanowires, *Nat. Phys.* **3**, 21 (2007).
- [31] S. S. P. Parkin, M. Hayashi, and L. Thomas, Magnetic domain-wall racetrack memory, *Science* **320**, 190 (2008).
- [32] S. S. P. Parkin and S.-H. Yang, Memory on the racetrack, *Nat. Nanotechnol.* **10**, 195 (2015).
- [33] D. A. Allwood, G. Xiong, M. D. Cooke, C. C. Faulkner, D. Atkinson, N. Vernier, and R. P. Cowburn, Submicrometer ferromagnetic NOT gate and shift register, *Science* **296**, 2003 (2002).
- [34] D. A. Allwood, G. Xiong, and R. P. Cowburn, Domain wall diodes in ferromagnetic planar nanowires, *Appl. Phys. Lett.* **85**, 2848 (2004).
- [35] D. A. Allwood, G. Xiong, C. C. Faulkner, D. Atkinson, D. Petit, and R. P. Cowburn, Magnetic domain-wall logic, *Science* **309**, 1688 (2005).
- [36] Y. Gaididei, V. P. Kravchuk, and D. D. Sheka, Curvature Effects in Thin Magnetic Shells, *Phys. Rev. Lett.* **112**, 257203 (2014).
- [37] V. P. Kravchuk, D. D. Sheka, A. Kákay, O. M. Volkov, U. K. Röbler, J. van den Brink, D. Makarov, and Y. Gaididei, Multiplet of Skyrmion States on a Curvilinear Defect: Reconfigurable Skyrmion Lattices, *Phys. Rev. Lett.* **120**, 067201 (2018).
- [38] J. A. Otálora, M. Yan, H. Schultheiss, R. Hertel, and A. Kákay, Curvature-Induced Asymmetric Spin-Wave Dispersion, *Phys. Rev. Lett.* **117**, 227203 (2016).
- [39] K. V. Yershov, V. P. Kravchuk, D. D. Sheka, and Y. Gaididei, Curvature-induced domain wall pinning, *Phys. Rev. B* **92**, 104412 (2015).
- [40] See Supplemental Material at <http://link.aps.org/supplemental/10.1103/PhysRevLett.123.077201> for details on experimental methods, analytical calculations, and main aspects of the model for curvilinear magnetic nanostripes, which includes Refs. [41–48].
- [41] F. Kronast, J. Schlichting, F. Radu, S. K. Mishra, T. Noll, and H. A. Dürr, Spin-resolved photoemission microscopy and magnetic imaging in applied magnetic fields, *Surf. Interface Anal.* **42**, 1532 (2010).
- [42] P. Fischer, Exploring nanoscale magnetism in advanced materials with polarized x-rays, *Mater. Sci. Eng. R* **72**, 81 (2011).
- [43] R. Hertel, Guided spin waves, in *Handbook of Magnetism and Advanced Magnetic Materials*, edited by H. Kronmüller, S. Parkin, M. Fähnle, S. Maekawa, and I. Zutic (John Wiley & Sons, Ltd., New York, 2007).
- [44] A. Kákay, E. Westphal, and R. Hertel, Speedup of FEM micromagnetic simulations with graphical processing units, *IEEE Trans. Magn.* **46**, 2303 (2010).
- [45] V. Slastikov, Micromagnetism of thin shells, *Math. Models Methods Appl. Sci.* **15**, 1469 (2005).
- [46] Y. Gaididei, A. Goussev, V. P. Kravchuk, O. V. Pylypovskyi, J. M. Robbins, D. D. Sheka, V. Slastikov, and S. Vasylykevych, Magnetization in narrow ribbons: Curvature effects, *J. Phys. A* **50**, 385401 (2017).
- [47] J. C. Slonczewski, Dynamics of magnetic domain walls, *AIP Conf. Proc.* **5**, 170 (1972).
- [48] A. A. Thiele, Steady-State Motion of Magnetic of Magnetic Domains, *Phys. Rev. Lett.* **30**, 230 (1973).
- [49] O. M. Volkov, F. Kronast, I. Mönch, M.-A. Mawass, A. Kákay, J. Fassbender, and D. Makarov, Experimental and theoretical study of curvature effects in parabolic nanostripes, *Phys. Status Solidi* **13**, 1800309 (2019).
- [50] R. H. Koch, J. G. Deak, D. W. Abraham, P. L. Trouilloud, R. A. Altman, Yu Lu, W. J. Gallagher, R. E. Scheuerlein, K. P. Roche, and S. S. P. Parkin, Magnetization Reversal in Micron-Sized Magnetic Thin Films, *Phys. Rev. Lett.* **81**, 4512 (1998).
- [51] B. C. Choi, M. Belov, W. K. Hiebert, G. E. Ballentine, and M. R. Freeman, Ultrafast Magnetization Reversal Dynamics Investigated by Time Domain Imaging, *Phys. Rev. Lett.* **86**, 728 (2001).
- [52] M. Kläui, P.-O. Jubert, R. Allenspach, A. Bischof, J. A. C. Bland, G. Faini, U. Rüdiger, C. A. F. Vaz, L. Vila, and C. Vouille, Direct Observation of Domain-Wall Configurations Transformed by Spin Currents, *Phys. Rev. Lett.* **95**, 026601 (2005).
- [53] O. Boulle, J. Vogel, H. Yang, S. Pizzini, D. de Souza Chaves, A. Locatelli, T. O. Menteş, A. Sala, L. D. Buda-Prejbeanu, O. Klein, M. Belmeguenai, Y. Roussigné, A. Stashkevich, S. M. Chérif, L. Aballe, M. Foerster, M. Chshiev, S. Auffret, I. M. Miron, and G. Gaudin, Room-temperature chiral magnetic skyrmions in ultrathin magnetic nanostructures, *Nat. Nanotechnol.* **11**, 449 (2016).
- [54] O. M. Volkov, D. D. Sheka, Y. Gaididei, V. P. Kravchuk, U. K. Röbler, J. Fassbender, and D. Makarov, Mesoscale Dzyaloshinskii-Moriya interaction: Geometrical tailoring of the magnetochirality, *Sci. Rep.* **8**, 866 (2018).
- [55] A. Fert, V. Cros, and J. Sampaio, Skyrmions on the track, *Nat. Nanotechnol.* **8**, 152 (2013).